Rheol Acta
DOI 10.1007/s00397-009-0420-6

ORIGINAL CONTRIBUTION

Extensional rheology of dilute polymer solutions in oscillatory cross-slot flow: the transient behaviour of birefringent strands

Simon J. Haward · Jeffrey A. Odell · Zhuo Li · Xue-Feng Yuan

Received: 30 June 2009 / Accepted: 15 December 2009

Abstract Birefringent strands are key to understanding polymeric non-Newtonian flows, especially in extension. Utilising microfluidic extensional flow oscillatory rheometry coupled with microvelocimetry (μ-PIV), we report experiments on the genesis, steady state and decay of such strands, together with rheological consequences. For closely monodisperse atactic polystyrene, we report massive effects of the polymer on flow even at low concentrations. The often observed startup "overshoot" in stress and birefringence is observed at unprecedented dilution and discussed in terms of the local strain rate. Strand decay shows pronounced hysteresis. These factors are most important in modelling real flows such as cyclic and capillary entrance flows. Even with the closely monodisperse and well-characterised samples used, residual polydispersity plays a vital role in flow behaviour.

Keywords Extensional flow · Flow-induced orientation · Elastic properties · Cross-slot · Birefringence · Polymer solution

Paper presented at the 5th Annual European Rheology Conference, April 15–17, 2009, Cardiff, UK.

S. J. Haward (✉) · J. A. Odell
HH Wills Physics Department, University of Bristol, Tyndall Avenue, Bristol BS8 1TL, UK
e-mail: s.j.haward@bristol.ac.uk

Z. Li · X.-F. Yuan
Manchester Interdisciplinary Biocentre and School of Chemical Engineering and Analytical Science, 131 Princess Street, Manchester M1 7DN, UK

Introduction

Extensional components are ubiquitous in flow fields since they are generated by a wide variety of flow geometries. Important examples include contraction/expansion and sink flows, bifurcations ('T' or 'Y' junctions), flow around obstacles and stagnation points (Pipe and McKinley 2009). Precisely such flow geometries occur in many important industrial, technological and biologically relevant processes including porous media flows (as in enhanced oil recovery and filtration), particle suspension/sedimentation, ink-jet printing, fibre spinning, biological flows of blood and mucin, among many others. Since such processes often inherently involve the flow of complex polymeric fluids, understanding the response of polymer molecules to such extensional flow fields is of fundamental importance.

Polymeric solutions display some remarkable non-Newtonian effects in extensional flows, a particularly dramatic example of which is the excess pressure drop observed in porous media flow (Marshall and Metzner 1967). It is this process that makes oil displacement by polymer flooding potentially viable. The cause of the pressure increase in porous media flow is likely to be the extension and alignment of polymer molecules in the flow field. Real and typical models of porous media consist of a random geometry of packed particles and contain all of the model geometries described above (contractions, bifurcations, etc). Cressely and Hocquart (1980, 1981) have shown through studies of flow-induced birefringence in poly(ethylene oxide) solutions that polymer molecules can become oriented in all of these types of model geometries.

De Gennes (1974) predicted that a sufficiently high velocity gradient (or strain rate) could cause

Published online: 06 January 2010

non-free-draining coiled polymer molecules to extend in a critical manner due to increasing frictional contact between polymer and solvent as the molecule uncoiled and became more free-draining. This runaway process could result in polymer molecules that were stretched to near their contour length. An additional effect of the increased polymer–solvent contact is an increasing molecular relaxation time in the extended state, resulting in hysteresis in the coil–stretch–coil cycle with strain rate. Similar predictions were also made by Hinch (1974).

In order for polymer molecules to be stretched in the manner suggested by De Gennes and Hinch, a dual condition must be satisfied. Firstly, the strain rate must be large enough to stretch the molecule. This means the strain rate, $\dot{\varepsilon}$, must exceed the molecular relaxation rate, $1/\tau$, so that the Deborah number, $De = \dot{\varepsilon} \times \tau > \sim 1$. Secondly, the strain rate must be applied for sufficient time for the molecule to accumulate strain. Flexible high-molecular-weight polymers may require strains ~100 or greater to be fully stretched. An increase of many orders of magnitude in the extensional viscosity would be expected when the molecules underwent the transition from coiled to fully stretched (e.g. Batchelor 1970). Note that numerical calculations by Larson and Magda (1989) predict that polymer molecules should stretch in flow provided that $De > \sim 0.5$, as opposed to 1.

The dual condition for full stretching is most readily satisfied in flows which contain a stagnation point. Since a stagnation point is a locality of zero fluid velocity but finite strain rate, a polymer molecule can effectively become trapped in the velocity gradient there for long enough to accumulate a high strain.

Various devices have been designed to generate easily observable and controllable stagnation point flows in the laboratory including the opposed jets (Frank et al. 1971) and the cross-slots (Scrivener et al. 1979). Experiments in these devices have tended to confirm the predictions of De Gennes and Hinch. Studies with well-characterised monodispersed polymer samples in theta solvents (atactic polystyrene in decalin) found that flow-induced birefringence at the stagnation point was observed only for strain rates, $\dot{\varepsilon}$, above a critical value, $\dot{\varepsilon}_c$, indicating the relaxation time $\tau = 1/\dot{\varepsilon}_c$, corroborating the predictions of De Gennes and Hinch (Carrington and Odell 1996; Carrington et al. 1997a, b). The birefringence was observed as a strand closely localised along exit streamlines passing close to the stagnation point where high fluid strains could be accumulated. The intensity of the birefringence rapidly increased with increasing strain rate to a plateau value consistent with that expected for very highly stretched polymer molecules. The increase in birefringence above $\dot{\varepsilon}_c$ was accompanied by an increase in the pressure drop measured across the device, indicating the expected increase in extensional viscosity. Spreading of the birefringence and extensional viscosity increase with strain rate was shown to be consistent with the narrow but finite molecular weight distribution of the polymer samples.

Cross-slot experiments that directly measured the dynamics of perfectly monodisperse fluorescently labeled DNA molecules uncoiling at a stagnation point have also shown that molecules can become highly stretched. However, the degree and rate of stretching are both highly dependant on the molecular conformation that develops in the early stages of uncoiling (Perkins et al. 1997; Smith and Chu 1998). Molecules were found to develop one of seven conformations: dumbbell, half-dumbbell, folded, kinked, uniform, coiled and extended. Such conformations are metastable, and over time, we would expect the extended or dumbbell configurations to evolve, given a sufficiently high strain rate. The average fractional molecular extension (end-to-end/contour length) reached a plateau of ~0.7 for high strain rates and high values of fluid strain. At high Deborah numbers of $De \sim 50$, stretching was found to be affine with the fluid for the initial ~25% of the extension.

Also, using fluorescently labeled DNA, Schroeder et al. (2003) have observed evidence of a small degree of conformation dependence of the molecular relaxation time or coil-stretch-coil hysteresis. The extent to which DNA is randomly coiled at equilibrium and is non-free-draining is perhaps open to conjecture.

Harlen et al. (1992) modelled the stretching of macromolecules in stagnation point flows using the finitely extendable nonlinear elastic, Peterlin approximation plus a non-constant diffusion coefficient (FENE-PCR) dumbbell model of Chilcott and Rallison (1988) with Deborah number-dependent nonlinear hydrodynamic friction. The results showed that the resulting strand of highly stretched molecules coming from a stagnation point could modify the flow field so as to cause a reduction in the strain rate within the strand. Remmelgas et al. (1999) compared the FENE-PCR model with a similar FENE, Peterlin approximation plus a configuration-dependent diffusion coefficient (FENE-PCD) model which has conformational-dependant hydrodynamic friction based on De Gennes' and Hinch's theories of coil–stretch hysteresis. The FENE-PCD model has a hydrodynamic friction that can increase as a coil stretches at fixed Deborah number. In cross-slot flow, both models resulted

in strands of highly stretched dumbbells following streamlines flowing away from the stagnation point, and both models showed flow modification within the strand. However, the FENE-PCD model resulted in a much larger degree of flow modification and in stretched strands of much greater length than the FENE-PCR model. The FENE-PCD model relaxed more slowly from the extended state due to the increase in hydrodynamic friction and resulted in better agreement with experimental observations of birefringence and flow perturbation than the FENE-PCR model (Gardner et al. 1982; Miles and Keller 1980).

However, even dumbbell models which incorporate variable hydrodynamic friction do not simulate the accumulation of macromolecular strain that is experimentally observed in cyclic periodic flows, e.g. by Cressely and Hocquart (1981) or Dyakonova et al. (1996).

Recent studies of highly elastic ultra-high-molecular-weight poly(acrylamide) solutions in cross-slot flows and numerical simulations based on simple viscoelastic fluid models have revealed low Reynolds number elastic instabilities which result in strong flow asymmetries near the stagnation point (Arratia et al. 2006; Poole et al. 2007).

Most stagnation point extensional flow experiments are performed under conditions of steady state; however, most real flows (e.g. pore entrances, pulsatile flows and flows along streamlines that pass close to (but not through a stagnation point) are transient in nature and/or result in limited fluid (and therefore macromolecular) strain. For such types of flow, it provides great insight to understand the genesis of macromolecular orientation and the resultant stretched strand structures and flow modification effects of the stretching polymer solution. Similarly, when the stretching component of the flow stops, or is removed from the flow field, it becomes important to understand how the stretching and orientation dies away.

Recent years in our laboratory have seen the development of a cross-slot-based device called the extensional flow oscillatory rheometer (EFOR; Odell and Carrington 2006). The EFOR uses piezoelectric micro-pumps to repeatedly oscillate a small volume of fluid through the stagnation point. This represents a significant advance due to the low volumes of polymer solution required, the fine control over the strain rate due to the use of accurate pumping and the ability to control the accumulation of fluid strain via control of the oscillation period. The EFOR can be used to assess shear and extensional viscosity by measuring the pressure drop, macromolecular strain (by measuring optical birefringence) and flow field modification using micro-particle image velocimetry (μ-PIV).

In this article, we make use of the EFOR's facilities to examine in detail the evolution in time of the structure and properties of an elastic strand from the transient start-up towards steady state and finally through relaxation following the cessation of flow. We use well-defined dilute and monodisperse solutions of atactic polystyrene (aPS) in dioctyl phthalate (DOP) which are close to θ conditions at room temperature. DOP is also a viscous solvent which, combined with the use of a microscale cross-slot, helps to minimise inertial contributions to the flow. Some interesting phenomena are reported, some of which are unexpected from dilute solutions.

Experimental

Apparatus

A schematic diagram of the EFOR is shown in Fig. 1. The apparatus is essentially as described in Carrington and Odell (1996). Fluid is pumped into one pair of opposing channels and out of the second pair, resulting in a stagnation point at the centre of the cross. The piezoelectric micro-pumps are driven by applying oscillating triangular voltage profiles of amplitude, V, and period, T, across them. This results in a linear displacement of each pump and hence a constant volume flow rate, Q, ($\propto V/T$) through each channel of the slot.

The superficial flow velocity, U, in each channel is given by:

$$U = \frac{Q}{dt} \tag{1}$$

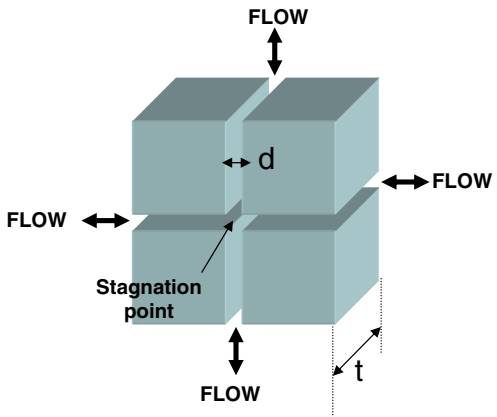

Fig. 1 Schematic diagram of the cross-slot flow cell of the EFOR

where d is the width of the channel and t is the depth of the channel. The nominal strain rate at the stagnation point, $\dot{\varepsilon}_{\text{nom}}$, is given by:

$$\dot{\varepsilon}_{\text{nom}} = \frac{2U}{d}. \tag{2}$$

The slots used in this study have a channel width of $d = 200$ μm and a depth of $t = 1$ mm, giving an aspect ratio of 5:1. The total length of each channel is $L = 1.2$ mm.

$\dot{\varepsilon}_{\text{nom}}$ is defined on the assumption that fluid accelerates from zero velocity at the stagnation point at the centre of the cross up to the superficial flow velocity, U, at the start of the exit channel of the cross, a distance $d/2$ away. This will be shown to be true for Newtonian fluids; however, it is not necessarily the case for polymeric solutions which can modify the flow field. In this experiment, we use μ-PIV to directly measure the flow field and determine the true strain rate, $\dot{\varepsilon}$, in the cross-slot.

The Deborah number, De, of the flow is the ratio of polymer relaxation time, τ, to characteristic flow time, $1/\dot{\varepsilon}$:

$$De = \dot{\varepsilon}\tau. \tag{3}$$

Inertial contributions to the flow are characterised by the Reynolds number, Re, defined by:

$$Re = \frac{\rho U D_{\text{h}}}{\eta_{\text{s}}} \tag{4}$$

where ρ is the solvent density, η_{s} is the solvent viscosity and D_{h} is the hydraulic diameter, given by $D_{\text{h}} = 2dt/(d+t)$. In our experiments, due to the microfluidic geometry and the viscous solvent, Re is always <4 and is generally <1.

The elasticity number, $El = De/Re$, gives a measure of the importance of elastic forces over inertial effects. In our experiments, El ranges from 2.5 to 9.5 depending on the polymer molecular weight.

The pressure difference, ΔP, in the cross-slots is measured as a function of strain rate across an inlet and an outlet channel, as shown schematically in Fig. 2. By disconnecting two of the pumps and simply measuring the pressure drop for flow of liquid around a corner of the cross-slot (ΔP_{shear}), we can measure the shear viscosity, η_{shear}, of the liquid. Assuming Poiseuille flow in a rectangular channel of total length $2L$:

$$\eta_{\text{shear}} = \frac{d^2 \Delta P_{\text{shear}}}{24 U L}. \tag{5}$$

Results for η_{shear} obtained with Eq. 5 agree well with results from a conventional ARES cone and plate rheometer.

By measuring the pressure drop with all four pumps running (ΔP_{total}), we can find the excess pressure drop due the extensional part of the flow field. Assuming the extensional viscosity in the birefringent strand, $\eta_{\text{ext}} >> \eta_{\text{shear}}$, and therefore dominates the excess pressure drop, we can obtain a measure of the extensional viscosity of the fluid comprising the elastic strand:

$$\eta_{\text{ext}} = \frac{\Delta P_{\text{total}} - \Delta P_{\text{shear}}}{\dot{\varepsilon}} \times \frac{d}{w}, \tag{6}$$

where w is the width of the birefringent strand (full width at half-maximum intensity).

The optics used for birefringence observation and measurement are also shown in Fig. 2. The light source is a stabilised 660-nm, 60-mW fibre-coupled diode laser from Oz Optics. The polariser and analyser are crossed

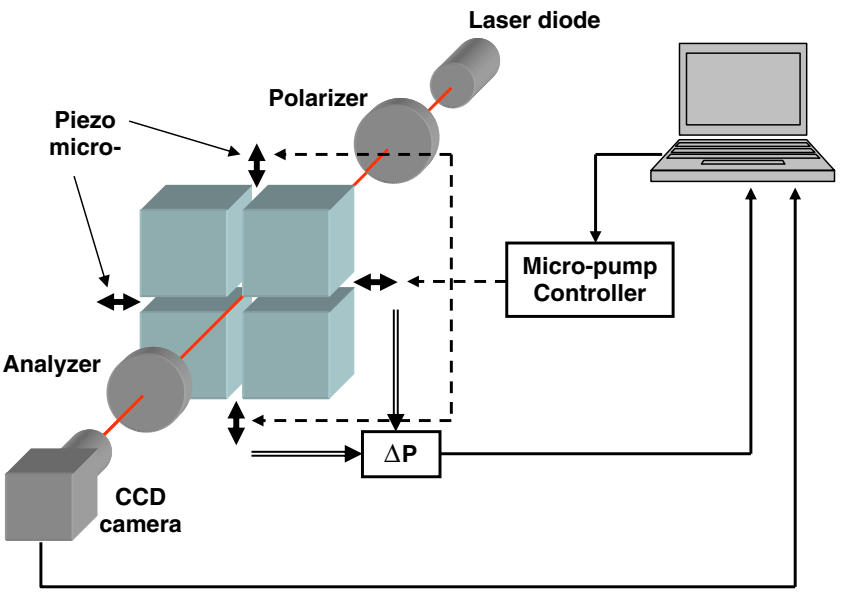

Fig. 2 Schematic diagram of the EFOR including micro-pump control, pressure measurement and optical line

at ±45° to the direction of the channels of the cross-slot, and a λ/4 plate was used to compensate for residual birefringence in the system. The CCD camera from Andor Technology is a deeply cooled (−80°C), very low-noise, high-quantum efficiency (~60%), 14-bit, 1,000 × 1,000 pixel camera capable of frame rates up to several hundreds per second.

Polymer solutions

Three aPS samples with molecular weights $M_p = 4.25 \times 10^6$, 6.9×10^6 and 10.2×10^6 Da from Polymer Laboratories were used in the study. The samples were closely monodisperse with $1.07 < M_w/M_n < 1.17$. DOP is a viscous ($\eta = 0.046$ Pa s) theta solvent for aPS at room temperature. Solutions of aPS in DOP were prepared at concentrations 0.005 wt.% $< c <$ 0.03 wt.% in the manner described by Carrington and Odell (1996). The overlap concentration, c^*, for the solutions is ~0.5 wt.% based on cubic packing of polymer coils at equilibrium (Graessley 1980); therefore, all our solutions are to be considered highly dilute.

For PIV experiments, solutions were seeded with fluorescent 1-μm diameter melamine resin tracer particles.

Results and discussion

Steady-state birefringence, viscometry and μ-PIV

Figure 3a shows a birefringent line observed in the cross-slots for the flow of a 0.03% solution of 6.9 M aPS in DOP at a nominal strain rate of 1,435 s^{-1}. Figure 3b shows a vector map of the flow field obtained using the μ-PIV system with the same polymer solution and strain rate as in Fig. 3a. In both Fig. 3a, b, left- and right-hand channels are the inlets and the top and

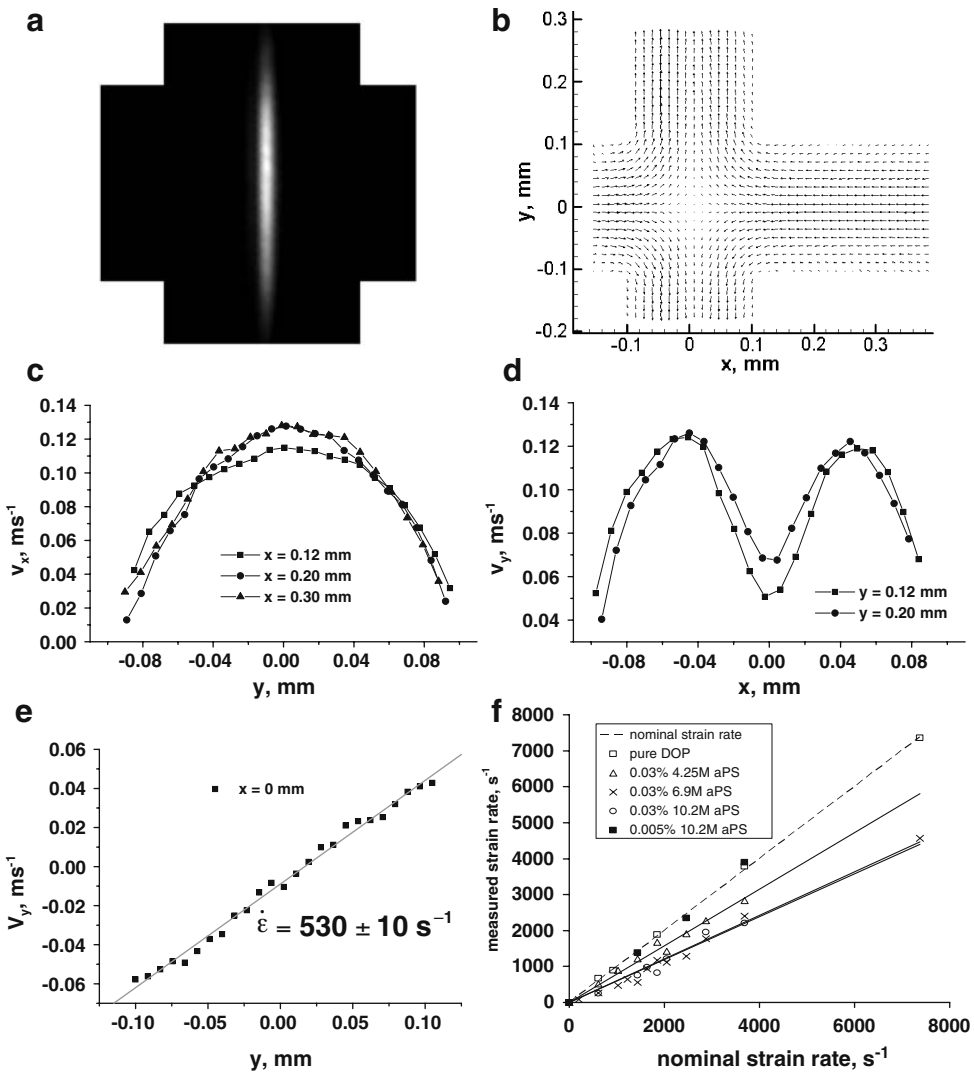

Fig. 3 **a** A birefringent line in the cross-slots observed with 0.03% 6.9 M aPS in DOP at a nominal strain rate of 1,435 s^{-1}. **b** Vector flow field obtained under the same conditions as **a**. **c** Velocity profiles across an inlet channel. **d** velocity profiles across an outlet channel. **e** Velocity along the central axis of the outlet channel showing the actual strain rate of 530 ± 10 s^{-1}. **f** Strain rate measured using μ-PIV compared with the nominal strain rate for various aPS/DOP solutions

bottom channels the outlets. It is evident from the vectors in Fig. 3b that the flow in the outlet channels is not Poiseuille-like since along the central axis of the outflow direction, corresponding to the location of the birefringent line, the vectors are shortened. This is observed more clearly by Fig. 3c, d which show velocity profiles across the right-hand inlet channel and the top exit channel, respectively. Across the inlet channel, we observe a Poiseuille-like parabolic flow profile, with zero flow velocity at the channel walls and maximum flow velocity in the centre of the channel. Across the outlet channel, the flow velocity profile is radically altered. Here, we have what looks like a "double Poiseuille" flow, with the flow velocity reaching minima at the channel walls and in the channel centre. It looks as though the channel has been divided down the centre into two narrower channels. It is apparent that the presence of a stretched elastic strand of polymer molecules can significantly modify the flow field even at this high dilution (here, $c \sim c^*/10$).

Figure 3e shows the flow velocity along the centreline of the outlet flow from the stagnation point, between the two outlet channel entrances at $y \pm 0.1$ mm. The gradient of Fig. 3e provides the value of the 'true' strain rate, $\dot{\varepsilon}$, that is actually experienced by polymer molecules within the birefringent as they flow away from the stagnation point. We find $\dot{\varepsilon} = 530 \pm 10\ \mathrm{s}^{-1}$, or just over 1/3 of $\dot{\varepsilon}_{\mathrm{nom}}$.

Micro-PIV has been used to experimentally determine $\dot{\varepsilon}$ as a function of $\dot{\varepsilon}_{\mathrm{nom}}$ for various aPS/DOP solutions and for the pure solvent using the same method as described for Fig. 3e. The results are presented in Fig. 3f, showing that $\dot{\varepsilon}$ is significantly modified from $\dot{\varepsilon}_{\mathrm{nom}}$ for 0.03% polymer solutions. For the 0.03% 4.25 M aPS sample, $\dot{\varepsilon} \sim 0.8 \times \dot{\varepsilon}_{\mathrm{nom}}$. The 0.03% 6.9 and 10.2 M aPS samples modify the flow to a similar degree and result in a strain rate of $\dot{\varepsilon} \sim 0.6 \times \dot{\varepsilon}_{\mathrm{nom}}$. The significance of this flow modification is particularly important to the determination of extensional viscosity in the cross-slot, defined in Eq. 6. If the true strain rate is not known and the nominal strain rate is used in the denominator of Eq. 6, this will lead to a significant underestimation of the extensional viscosity.

It is important to note in Fig. 3f that the strain rate measured for pure DOP between the outlet channel entrances does not significantly deviate from the nominal value, and neither does the strain rate measured for a 0.005% ($c \sim c^*/100$) solution of 10.2 M aPS. This indicates that the 0.005% solutions may be considered to be 'truly' dilute in the sense that they do not cause modifications to the flow field even when highly stretched.

Figure 4a shows the birefringence (normalised by the maximum measured value) as a function of $\dot{\varepsilon}$ for 0.005% solutions of aPS of various molecular weights in DOP. Differentiating the curves in Fig. 4a, we can find maxima corresponding to the strain rate at which the peak of the molecular weight distribution stretches. The inverse of the strain rate at this peak gives a value for the relaxation time of the peak of the molecular weight distribution. The coil–stretch relaxation times, τ_{c-s}, determined in this way are plotted against M_p in Fig. 4b. They clearly follow the $M^{1.5}$ relationship expected for the relaxation time in a theta solvent. The

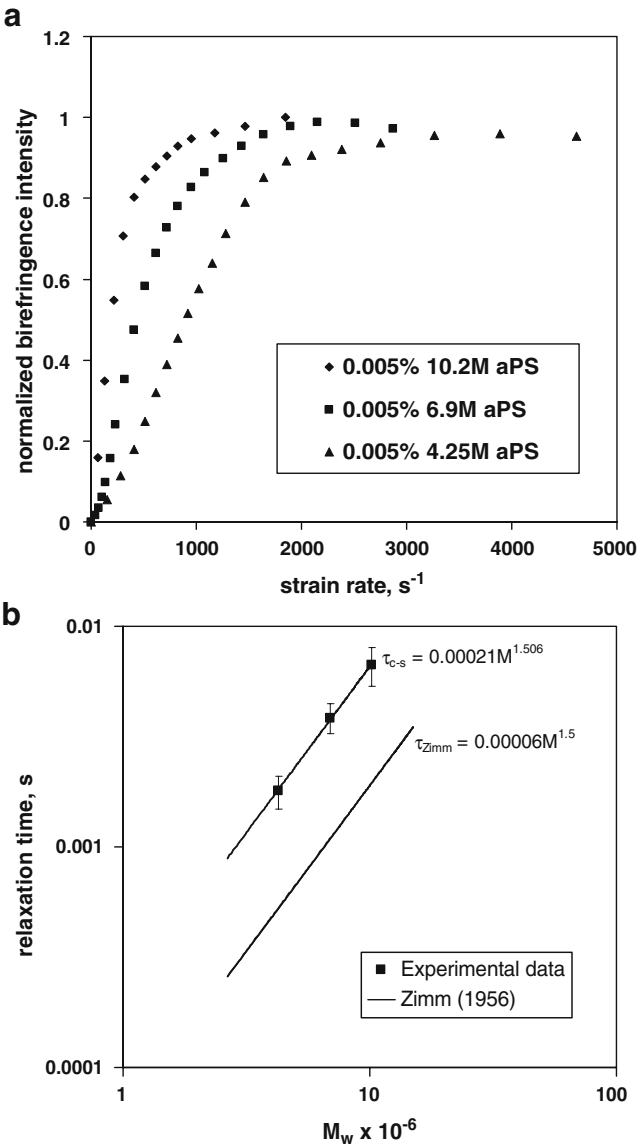

Fig. 4 **a** Normalised steady-state birefringence measured at the stagnation point as a function of strain rate. **b** Experimental relaxation times determined from the curves in **a**, showing a Zimm relationship

solid line represents the relaxation time obtained from Zimm (1956), calculated according to:

$$\tau_{\text{Zimm}} = \frac{0.2\eta_s R_g^3}{K_B T} \tag{7}$$

where R_g is the unperturbed radius of gyration, K_B is Boltzmann's constant and T is the temperature. The relaxation times are summarised in Table 1, showing reasonably close agreement between experimental and calculated values. If the theory of Larson and Magda (1989) is followed, then the experimental values of τ_{c-s} will be reduced by a factor of 2 and will be much closer to the theoretical Zimm values. The small discrepancy is most likely explained by a slight deviation from theta conditions in the experiment (due to temperature), resulting in a small increase in R_g.

Figure 5 shows experimentally measured birefringence and extensional viscosity data plotted against the Deborah number, *De*, calculated using the measured strain rate, $\dot{\varepsilon}$, and the measured relaxation time, τ, reported in Table 1. The data presented are for 0.005% and 0.03% 6.9 M aPS solutions after steady state has been achieved. The birefringence is measured at the stagnation point of the cross-slot.

It is clear that both the birefringence and the extensional viscosity begin to increase at a similar value of *De*. Broadly, this value is $De \sim 0.5$–1, although there is some spread in the data which we attribute to the small but finite polydispersity of the molecular weight distribution.

The sigmoidal-shaped birefringence curves in Fig. 5a are typical of those observed for stretching of solutions of flexible polymers of low polydispersity index (Carrington and Odell 1996; Carrington et al. 1997a, b). The theoretical maximum birefringence for a solution of fully stretched polystyrene molecules is 0.078.*c*, where *c* is the polymer concentration (Carrington et al. 1997a, b). Using the Treloar model of rubber elasticity, based on an approximation to the inverse Langevin function and the optical properties of strained networks, we can find an estimate of the fractional molecular extension, β, the ratio of end-to-end separation to contour length (Treloar 1975; Carrington et al 1997a, b). At high *De*, the extension ratio tends to a value of $\beta \sim 0.6$–0.7. This is consistent with the ensemble

Table 1 Relaxation times of aPS in DOP

$M_p \times 10^{-6}$(gmol^{-1})	τ_{c-s}(ms)	τ_{Zimm}(ms)
4.25	1.8 ± 0.3	0.5
6.9	3.9 ± 0.6	1.1
10.2	6.7 ± 1.3	2.0

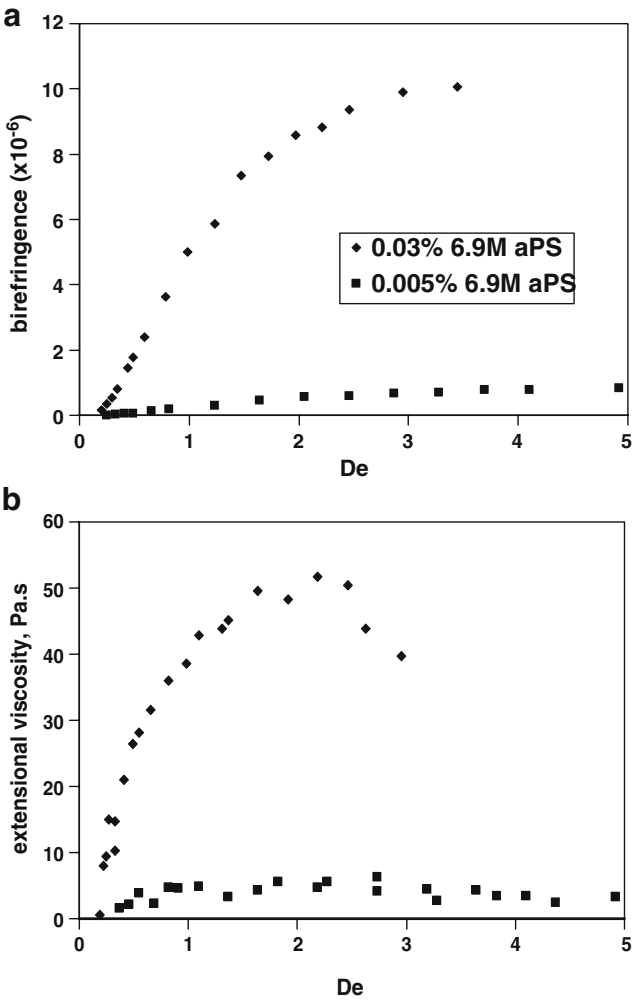

Fig. 5 **a** Steady-state birefringence. **b** Extensional viscosity as a function of Deborah number for solutions of 6.9 M aPS in DOP

average value reported by Perkins et al. (1997) with fluorescently labeled DNA molecules at high *De* and for large fluid strains.

Figure 5b shows the extensional viscosity, calculated according to Eq. 6, as a function of strain rate. We have measured the width of the birefringent line, w, to be ~1/20th of the width of the channel, d, independent of strain rate or concentration. We see that the extensional viscosity increases rapidly with strain rate to a peak value before a plateau and a slight reduction. The shear viscosities of the polymer solutions are essentially equal to the solvent viscosity of $\eta_{DOP} \sim 0.046$ Pa s. From Fig. 5b, we can estimate the Trouton ratio, $Tr = \eta_{ext}/\eta_{shear}$, for the 0.03% aPS solution to be $Tr \sim 1{,}000$.

According to the slender body theory of Batchelor (1970), we should expect $Tr \sim 11{,}000$ from this 0.03% solution (if it were perfectly monodisperse and fully

stretched to its contour length). However, our value of $Tr \sim 1{,}000$ compares fairly well with values found with similarly dilute and high-molecular-weight aPS solutions in filament stretching rheometers (e.g. Gupta et al. 2000; Li et al. 2000; Hsieh and Larson 2004). Hsieh and Larson found that their experimental values of Trouton ratio reached plateaus of ~1/4 of the value expected (in this case from Brownian dynamics simulations with hydrodynamic interaction parameters obtained from Batchelor's theory). They explained the discrepancy as being due to polymer chain scission. However, in our experiments, we are confident there is no chain scission which would be immediately noticeable as a reduction in the birefringence.

In Batchelor's theory, Tr depends on the cube of the contour length and is only weakly dependent on the molecular diameter. Given an extension ratio of 0.7, we might therefore expect $Tr \sim 11{,}000 \times 0.7^3 \sim 3{,}800$. However, when chains are not fully extended, the residual springiness will mean they will not be well modelled by the inextensible rods assumed by Batchelor. Additionally, we note that there is relaxation of macromolecular strain as the stretched polymer strand extends away from the stagnation point (see Figs. 6 and 7), meaning that the average extension ratio along the whole strand will be somewhat lower than the value of ~0.7 measured at the stagnation point. Gupta et al, Li et al and Hsieh and Larson report experimental values of Trouton ratio that scale linearly with molecular weight or contour length. This behaviour is captured by a FENE dumbbell model with hydrodynamic interactions (Gupta et al. 2000), but not by the Brownian dynamics simulations of Hsieh and Larson (2004).

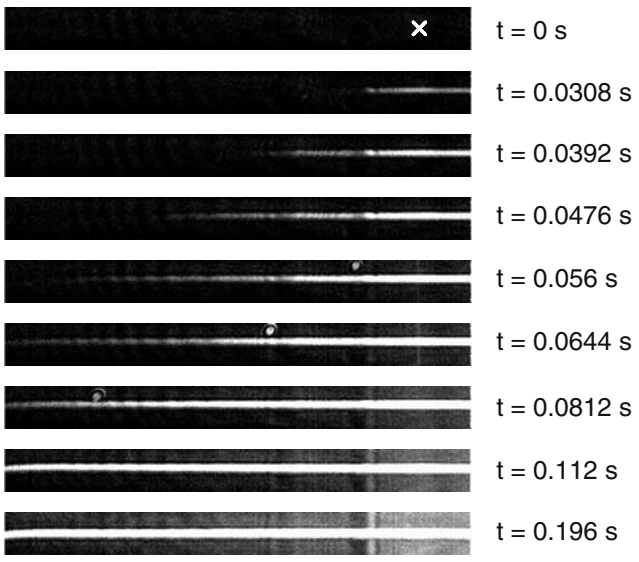

Fig. 6 Development of a birefringent line from initial start up until steady state. 0.03% 10.2 M aPS/DOP at a strain rate of 3,69 s^{-1}, $De = 2.5$. The *white "x"* marks the stagnation point

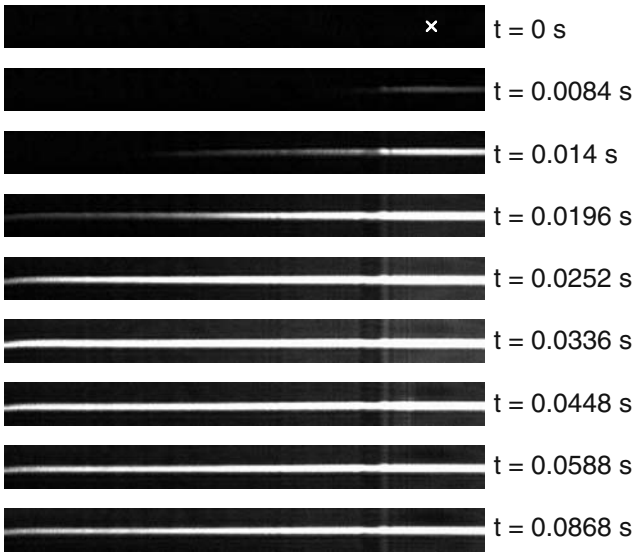

Fig. 7 Development of a birefringent line from initial start up until steady state. 0.03% 10.2 M aPS/DOP at a strain rate of 2,216 s^{-1}, $De = 14.8$. The *white "x"* marks the stagnation point

Flow start-up

Figure 6 shows the growth and development of a birefringent line in the cross-slot for a 0.03% solution of 10.2 M aPS in DOP at $De \sim 2.5$. The experiment was performed using a cylindrical lens to spread the laser light along one of the channels of the cross-slot. Using the camera capture software to select a 'letter box'-shaped region of interest around the exit channel and putting pixels into 2 × 2 bins enabled the capture rate to be increased to ~360 fps (frames per second). Frame capture was initiated before the flow was started, so the increase in birefringence was recorded from zero time. The length, breadth and intensity of the line are observed to increase rapidly until a steady state is reached after ~0.2 s. The fully developed line then extends the entire length of the exit channel, which is 1.2 mm, although the birefringence intensity clearly decreases with distance from the stagnation point, indicating some degree of strain relaxation. The average rate of growth of the birefringent line along the channel from the stagnation point to the end of the channel is ~0.03 ms^{-1}. This is about half of the superficial flow velocity, roughly consistent with the flow modification reported in Fig. 3f, showing $\dot{\varepsilon} \sim 0.6 \times \dot{\varepsilon}_{nom}$ for this solution.

Figure 7 shows a similar time sequence as Fig. 6, but this time for $De \sim 15$. In this case, we notice similar initial growth of the birefringent line; however,

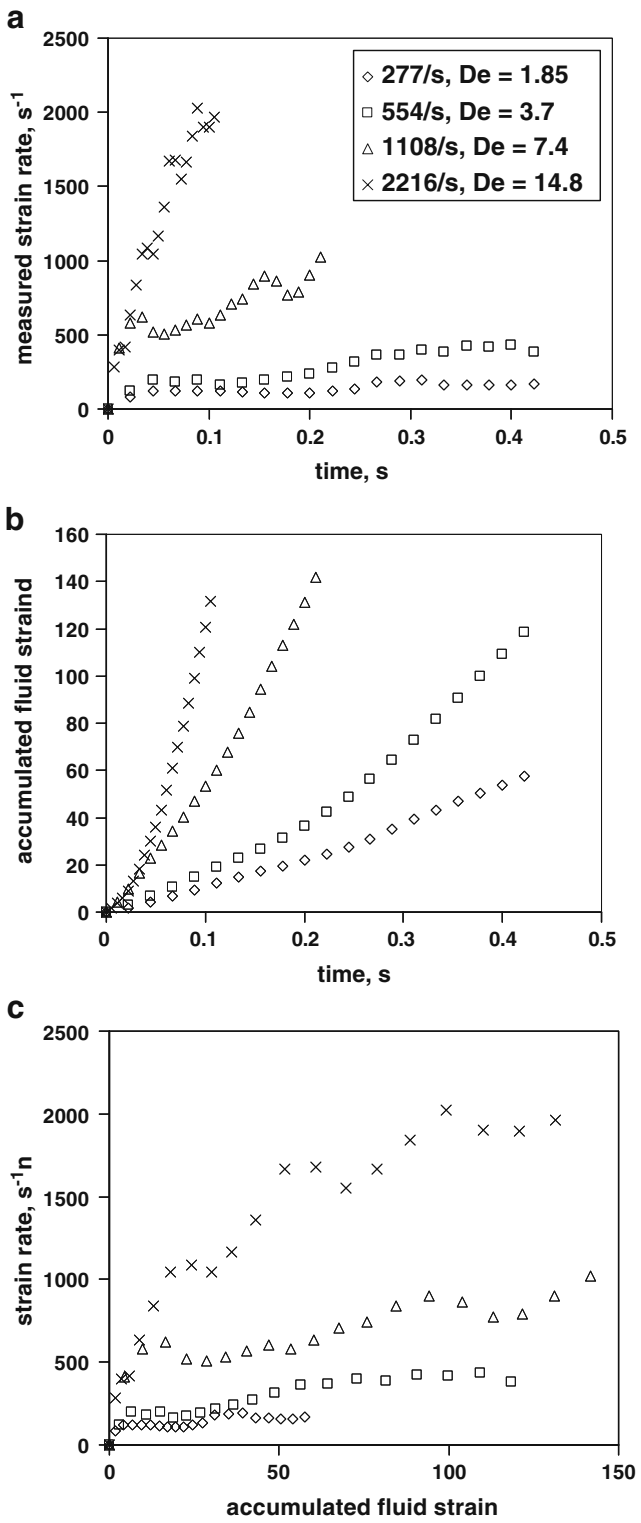

Fig. 8 μ-PIV data captured during flow start-up for 0.03% 10.2 M aPS in DOP for various steady-state values of strain rate/*De*

a maximum in intensity is reached after ∼0.034 s, after which the intensity diminishes to its steady state value after ∼0.1 s.

Figure 8a shows the results of time resolved μ-PIV measurements made on the 0.03% 10.2 M aPS solution during the initial flow startup for various steady-state values of strain rate. Using the measured strain rate as a function of time, it is possible to calculate how the fluid strain at the stagnation point accumulates with time; this is shown in Fig. 8b. For small times, the rate of strain accumulation increases with time until it reaches a near constant value (i.e. fluid strain ∝ time) after a time equivalent to ∼5% of a pump cycle period. In the solvent, 90% of the superficial strain rate was achieved after ∼3% of a pump cycle period. The difference is most likely to be due to the gradual accumulation of macromolecular strain in the birefringent strand progressively affecting the flow field. In Fig. 8c, we show how the strain rate varied with the accumulated fluid strain.

In Fig. 9, we show the birefringence measured at the stagnation point (normalised by the theoretical maximum value) as a function of the accumulated fluid strain. For high *De* flows, we see an overshoot in birefringence before the steady-state value is reached. Below $De \sim 4$, the overshoot has essentially vanished, although the steady-state value of birefringence remains the same as for higher *De*.

Using the Treloar model of rubber elasticity, we have estimated the birefringence we would expect from the polymer solutions if all the molecules deformed affinely with the fluid. The results are plotted on Fig. 9 as solid lines. We find that the actual measured birefringence increases much more rapidly than the affine prediction. This is most likely to be due to the assumption in the Treloar model that polymer deformation occurs by increasing the end-to-end separation of chains. Birefringence provides a measure of segmental orientation, and it is clear that in the early stages of deformation, increasing the end-to-end separation does not necessarily result in a large degree of segmental orientation. However, for very tightly coiled molecules, such as high-molecular-weight aPS in DOP, a far more likely mode of deformation upon exposure to an extensional flow field is that the entire coil becomes squashed and stretched. This would result in a far larger degree of local segmental orientation whilst not necessarily causing a significant increase in end-to-end distance.

Upon continued exposure to the extensional flow field, we can assume that polymer chains will uncoil and increase their end-to-end separation. Therefore, we can apply the Treloar model to the steady-state birefringence values to obtain extension ratios for both the 10.2 and 6.9 M aPS molecules of $\beta \sim 0.6$–0.7, consistent with Perkins et al. (1997), as before.

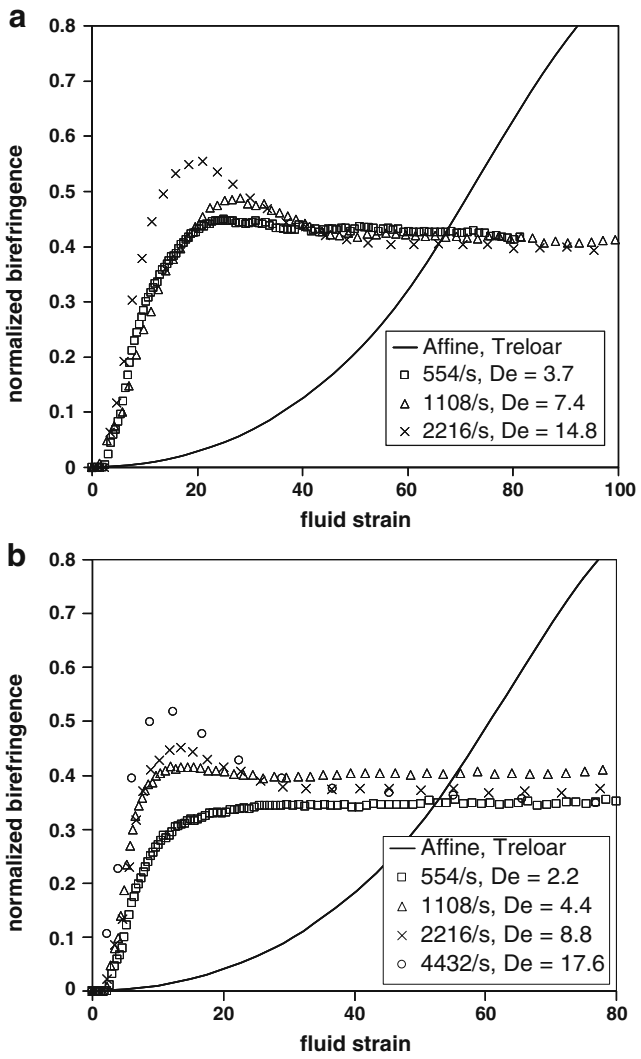

Fig. 9 Development of birefringence with increasing fluid strain from initial start-up until steady state: **a** 0.03% 10.2 M aPS/DOP, **b** 0.03% 6.9 M aPS/DOP. The *solid lines* show calculated curves according to Treloar rubber elasticity theory for affine deformation of the polymer with the fluid

Overshoots in flow-induced birefringence during start-up have been observed previously, e.g. by Geffroy and Leal (1992) and Wang et al. (1994) in a co-rotating two-roll mill; however, these were made using highly concentrated polymer solutions. Experimental studies with dilute monodisperse polystyrene solutions in the two-roll mill showed no evidence of a birefringence overshoot (Harisson et al. 1998, 1999), although simulations with Chilcott–Rallison FENE-CR dumbbells did predict an overshoot. The overshoot in the simulation was attributed to the complex interaction between polymer conformation and resulting flow field modification (Harisson et al. 1999). As the dumbbell stretched, the flow modification increased towards a steady state, which was followed by a slight relaxation of the dumbbell extension due to the flow becoming weaker.

However, in our experiments, we observe no overshoot in the measured strain rate to correspond with the birefringence overshoot. Indeed, the strain rate continues to increase even after the birefringence overshoot has passed and the steady-state value of birefringence has been reached. This would not be expected on the basis of Harrison's suggestion for the overshoot mechanism.

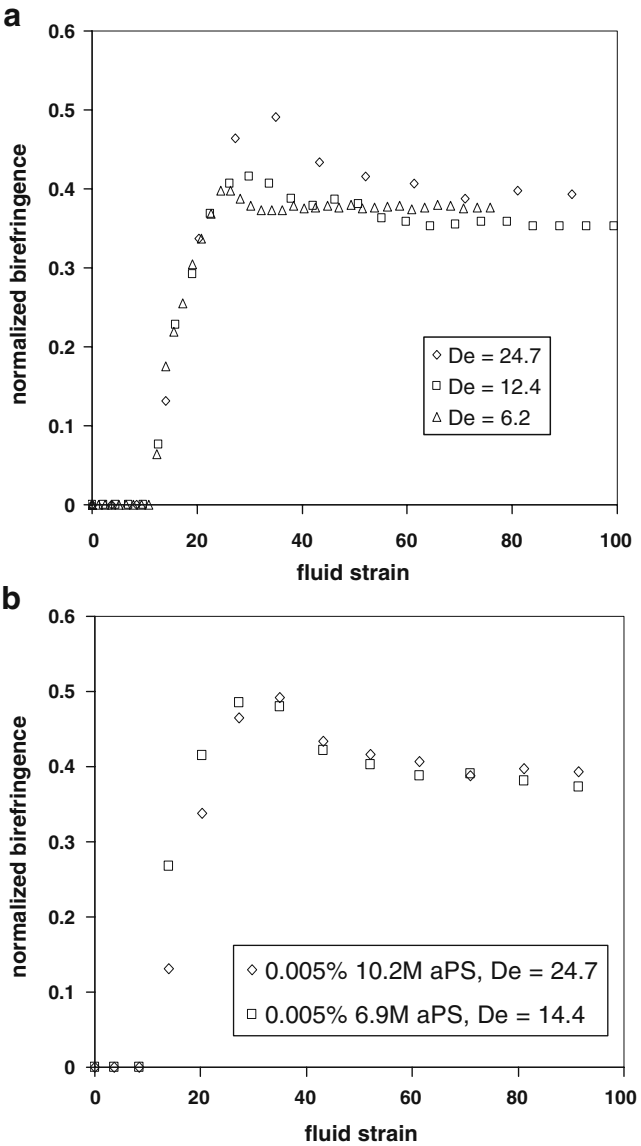

Fig. 10 Development of birefringence with increasing fluid strain from initial start-up until steady state: **a** 0.005% 10.2 M aPS/DOP, **b** 0.005% 6.9 M and 10.2 M aPS/DOP

In fact, we have even observed overshoots in the birefringence with aPS solutions at concentrations of 0.005% (see Fig. 10), for which we find no discernible flow modification at all. We believe this is the first time that experimentally observed birefringence overshoots have been reported at such low polymer concentrations (here, $c/c^* \sim 0.01$).

We note that in our start-up and steady-state experiments with dilute aPS/DOP solutions, we have not observed the elastic instabilities and flow asymmetries reported by Arratia et al. (2006) and modelled by Poole et al. (2007). We believe that the results of Arratia et al. may be explained by the extremely highly elastic nature of the polymer solution they studied, which was a highly polydisperse polyacrylamide of $M_w = 18 \times 10^6$ Da at 0.02 wt.% concentration in a very viscous solvent.

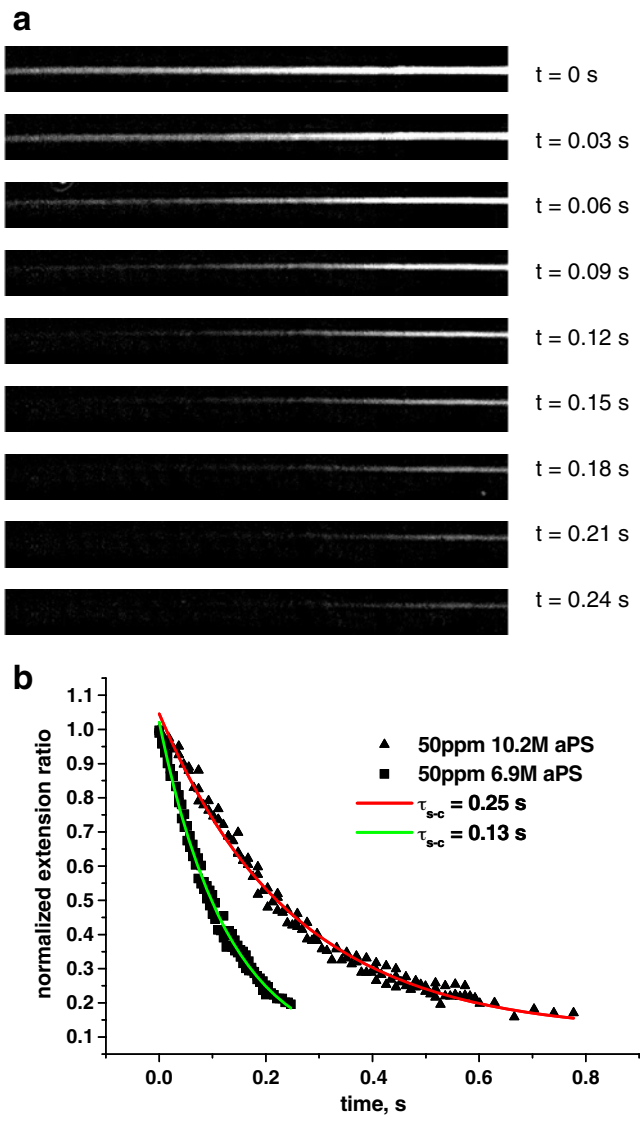

Fig. 11 **a** Decay of birefringence with time for a 0.005% solution of 10.2 M aPS/DOP. **b** Decay of molecular extension over time fitted with exponential decay curves with time constants τ_{s-c}

Birefringence decay

Figure 11a shows a time sequence of birefringence images obtained with a 0.005% solution of 10.2 M aPS in DOP. The polymer solution was stretched at a strain rate of $\dot{\varepsilon} = 923\ s^{-1}$ ($De \sim 6.2$) until the steady state was reached. At this point ($t = 0$ s), the flow was suddenly halted by instantaneously stopping the piezo micropumps. Images were captured continuously at a rate of ~270 fps as the birefringence decayed away. Figure 11b shows the normalised fractional molecular strain as a function of time, determined from the birefringence measured at the stagnation point. The data are well fitted by a single exponential decay of the form $\beta = A + Be^{-t/\tau_{s-c}}$, where A and B are constants and τ_{s-c} is the stretch–coil relaxation time. We find a value of $\tau_{s-c} = 0.25 \pm 0.01$ s for the decay from the stretched to the coiled state for the 10.2 M aPS sample and $\tau_{s-c} = 0.13 \pm 0.01$ s for the 6.9 M aPS sample. These are both ~35 times greater than τ_{c-s}, determined for the coil–stretch transition and is clear evidence of the coil–stretch–coil hysteresis predicted by De Gennes (1974) and Hinch (1974).

Conclusions

This study has shown that the combination of EFOR with microvelocimetry (μ-PIV) is very powerful for understanding transient extensional and periodic flow behaviour. EFOR allows strain rate and strain to be separately varied in a clean microfluidic environment. μ-PIV permits fast reproducible results to be obtained with a spatial resolution of 3 μm. The often reported birefringence and stress overshoot at the inception of flow is observed, but in our experiment, the origin is not an overshoot in the local strain rate.

In steady state, this substantially elastic strand leads to a dramatic increase in apparent extensional flow velocimetry, with Trouton ratios as high as 1000, even at high dilutions of $<0.1c^*$. We find that dilution to $0.01c^*$ is sufficient to obviate flow perturbation effects.

It is clear that even for these closely monodisperse aPS polymers ($M_w/M_n \sim 1.1$), polydispersity plays an important role and results in major departures from "ideal" behaviour, both as a result of the major flow

perturbation of the high tail and the progressive or incomplete stretching of the low tail at moderate Deborah numbers. It is often not appreciated that such "monodisperse" polymers typically contain a substantial fraction of molecular weights spanning more than a decade. If this is true for such materials, then it is vital to understand the behaviour of commercial polydisperse materials where molecular weight species can span several decades.

Finally, it is shown that there is a strong hysteresis between the coil→stretch and the stretch→coil relaxation process, the relaxation time being ∼35 times greater than the stretching characteristic time. This can be partially modelled by the FENE-PCR and FENE-PCD dumbbell models which incorporate hydrodynamic hysteresis. However, even these models do not account for the accumulation of strain in successive cycles of periodic flows (Dyakonova et al. 1996) in any flow where symmetry is expected, which is of particular importance in understanding dilute porous media flow (Marshall and Metzner 1967). However, the strand development and overshoot breaks the presumed symmetry of such flows and, from an understanding of the non-Newtonian nature and dynamics of strand development, modelling of such flows will emerge.

Acknowledgement We gratefully acknowledge the support of the Engineering and Physical Sciences Research Council (EPSRC) of the U.K.

References

Arratia PE, Thomas CC, Diorio J, Gollub JP (2006) Elastic instabilities of polymer solutions in cross channel flow. Phys Rev Lett 96:144502

Batchelor GK (1970) Slender-body theory for particles of arbitrary cross-section in Stokes flow. J Fluid Mech 44:419–440

Carrington SP, Odell JA (1996) How do polymers stretch in stagnation point extensional flow-fields? J Non-Newton Fluid Mech 67:269–283

Carrington SP, Tatham JP Odell JA, Saez AE (1997a) Macromolecular dynamics in extensional flows: 1. Birefringence and viscometry. Polymer 38:4151–4164

Carrington SP, Tatham JP Odell JA, Saez AE (1997b) Macromolecular dynamics in extensional flows: 2. The evolution of molecular strain. Polymer 38:4595–4607

Chilcott MD, Rallison JM (1988) Creeping flow of dilute polymer solutions past cylinders and spheres. J Non-Newton Fluid Mech 29:381–432

Cressely R, Hocquart R (1980) Biréfringence d'écoulement localisée iduite à l'arrière d'obstacles. Opt Acta 27:699–711

Cressely R, Hocquart R (1981) Extension and relaxation of high macromolecules in oscillatory elongational flow using flow birefringence. Polymer Prepr 22:120–121

De Gennes PG (1974) Coil–stretch transition of dilute flexible polymers under ultrahigh velocity gradients. J Chem Phys 60:5030–5042

Dyakonova NE, Odell JA, Brestkin YV, Lyulin AV, Saez AE (1996) Macromolecular strain in periodic models of porous media flows. J Non-Newton Fluid Mech 67:285–310

Frank FC, Keller A, Mackley MR (1971) Polymer chain extension produced by impinging jets and its effect on polyethylene solution. Polymer 12:467–473

Gardner K, Pike ER, Miles MJ, Keller A, Tanaka K (1982) Photon-correlation velocimetry of polystyrene solutions in extensional flow fields. Polymer 23:1435–1442

Geffroy E, Leal LG (1992) Flow birefringence studies of a concentrated polystyrene solution in a two-roll mill. 1. Steady flow and startup of steady flow. J Polym Sci Part B Polym Phys 30:1329–1349

Graessley WW (1980) Polymer chain dimensions and the dependence of viscoelastic properties on concentration, molecular weight and solvent power. Polymer 21:258–262

Gupta RK, Nguyen DA, Sridhar T (2000) Extensional viscosity of dilute polystyrene solutions: effect of concentration and molecular weight. Phys Fluids 12:1296–1318

Harisson G, Remmelgas J, Leal LG (1998) The dynamics of ultradilute polymer solutions in transient flows: comparison of dumbbell-based theory and experiments. J Rheol 42:1039–1058

Harisson G, Remmelgas J, Leal LG (1999) Comparison of dumbbell-based theory and experiment for a dilute polymer solution in a corotating two-roll mill. J Rheol 43:197–218

Harlen OG, Hinch EJ, Rallison JM (1992) Birefringent pipes: the steady flow of a dilute polymer solution near a stagnation point. J Non-Newton Fluid Mech 44:229–265

Hinch EJ (1974) Mechanical models of dilute polymer solutions for strong flows with large polymer deformations. Polymeres et Lubrification, Colloques Internationaux du CNRS 233:241–247

Hsieh C-C, Larson RG (2004) Modeling hydrodynamic interaction in Brownian dynamics: simulations of extensional and shear flows of dilute solutions of high molecular weight polystyrene. J Rheol 48:995–1021

Larson RG, Magda JJ (1989) Coil–stretch transitions in mixed shear and extensional flows of dilute polymer solutions. Macromolecules 22:3004–3010

Li L, Larson RG, Sridhar T (2000) Brownian dynamics simulations of dilute polystyrene solutions. J Rheol 44:291–322

Marshall RJ, Metzner AB (1967) Flow of viscoelastic fluids through porous media. Ind Eng Chem Fundam 6:393–400

Miles MJ, Keller A (1980) Conformational relaxation time in polymer solutions by elongational flow experiments 2. Preliminaries of further developments: chain retraction; identification of molecular weight fractions in a mixture. Polymer 21:1295–1298

Odell JA, Carrington SP (2006) Extensional flow oscillatory rheometry. J Non-Newton Fluid Mech 137:110–120

Perkins TT, Smith DE, Chu S (1997) Single polymer dynamics in an elongational flow. Science 276:2016–2021

Pipe CJ, McKinley GH (2009) Microfluidic rheometry. Mech Res Commun 36:110–120

Poole RJ, Alves MA, Oliveira PJ (2007) Purely elastic flow asymmetries. Phys Rev Lett 99:164503

Remmelgas J, Singh P, Leal LG (1999) Computational studies of nonlinear elastic dumbbell models of Boger fluids in a cross-slot flow. J Non-Newton Fluid Mech 88:31–61

Schroeder CM, Babcock HP, Shaqfeh ESG, Chu S (2003) Observation of polymer conformation hysteresis in extensional flow. Science 301:1515–1519

Scrivener O, Berner C, Cressely R, Hocquart R, Sellin R, Vlachos NS (1979) Dynamical behaviour of drag-reducing polymer solutions. J Non-Newton Fluid Mech 5:475–495

Smith DE, Chu S (1998) Response of flexible polymers to sudden elongational flow. Science 281:1335–1340

Treloar LKG (1975) The physics of rubber elasticity, 3rd edn. Clarendon, Oxford

Wang JJ, Yavich D, Leal LG (1994) Time-resolved velocity gradient and optical anisotropy in linear flow by photon correlation spectroscopy. Phys Fluids 6:3519–3534

Zimm BH (1956) Dynamics of polymer molecules in dilute solution: viscoelasticity, flow birefringence and dielectric loss. J Chem Phys 24:269–278